ECMWF – ARM Report Series

2. *A dual mass flux framework for boundary layer convection. Part I: Transport*

Roel A. J. Neggers, Martin Köhler, Anton C. M. Beljaars

European Centre for Medium-Range Weather Forecasts
Europäisches Zentrum für mittelfristige Wettervorhersage
Centre européen pour les prévisions météorologiques à moyen terme

Series: ECMWF - ARM Report Series

A full list of ECMWF Publications can be found on our web site under:
http://www.ecmwf.int/publications/

Contact: library@ecmwf.int

European Centre for Medium Range Weather Forecasts
Shinfield Park, Reading, RG2 9AX, England

ECMWF - ARM Report Series No. 2

A dual mass flux framework for boundary layer convection. Part I: Transport

Roel A. J. Neggers, Martin Köhler, Anton C. M. Beljaars

March 6, 2007

ARM – Atmospheric Radiation Measurement

Abstract

The eddy diffusivity - mass flux (EDMF) approach for turbulent transport in well-mixed layers is extended into the modeling of shallow cumulus convection. Model complexity is enhanced to enable representation of conditionally unstable cloud layers that are flexibly coupled to the mixed layer. This significantly expands the range of applicability of EDMF, in principle including all major regimes of boundary layer convection and transitions between those. The treatment of subgrid transport and clouds is integrated by parameterizing both in terms of the same turbulent joint-distribution. This potentially skewed distribution is reconstructed using an ensemble of resolved updrafts, rising from the surface layer. Part I of this study concerns the formulation of this multiple updraft framework. A key new ingredient is the application of flexible area partitioning in the updraft ensemble, which is determined by the coupling between cumulus clouds and the sub-cloud mixed layer. This is achieved by defining and resolving two specific groups of updrafts; dry mixed-layer updrafts that never reach their lifting condensation level, and moist updrafts that condense and become positively buoyant cumulus clouds. This technique facilitates the representation of gradual transitions to and from shallow cumulus convection, and implicitly represents the impact of cloud base transition layer stability on cumulus transport. Other upgrades include i) flexible updraft entrainment rates, ii) stability feedbacks on the vertical structure of cloudy mass flux, and iii) the introduction of an entrainment efficiency closure for transport into the cumulus inversion. Impacts of these new components on boundary layer structure and equilibration are assessed.

1 Introduction

Shallow cumulus convection was first represented in the Integrated Forecasting System (IFS) of the European Centre for Medium-range Weather Forecasts (ECMWF) by Tiedtke et al. (1988), reporting large but mostly favourable impacts on global model climate. Since its introduction, the basic structure of the shallow cumulus scheme has not changed significantly. However, biases in the IFS climate have recently been diagnosed that are related to the representation of shallow cumulus convection. A recent intercomparison study of cloud representation in general circulation models (GCM) for the north-east Pacific (Siebesma et al., 2004) illustrates that the current IFS typically predicts too much cloudiness in the subtropical marine Tradewind regions, but too little in the stratocumulus subsidence areas. Evaluation against observations at the Southern Great Plains (SGP) site of the Atmospheric Radiation Measurement (ARM) program (Stokes and Schwartz, 1994; Ackerman and Stokes, 2003) has revealed that the occurrence of summertime shallow cumulus is underestimated (Cheinet, 2004), and that the onset of precipitating convection occurs too early (Mace et al., 1998; Betts and Jakob, 2002). Further detailed evaluation of model physics against large-eddy simulation (LES) has traced some of these shortcomings to individual model components. For example, Neggers et al. (2004) illustrated that the moist static energy convergence closure used in the ECMWF model predicts too vigorous cumulus mass fluxes, directly causing too fast deepening cloud and sub-cloud layers and a too fast hydrological cycle.

These issues have motivated a critical reassessment of the representation of the planetary boundary layer (PBL) in IFS. A recent structural model upgrade has been the introduction of the Eddy Diffusivity Mass Flux framework (EDMF, Siebesma and Teixeira, 2000; Siebesma et al., 2007) in IFS, as documented by Köhler (2005) and Tompkins et al. (2004). This method combines diffusive and advective models in the parameterization of turbulent transport, thus making use of the different nature of both techniques. The EDMF scheme as currently operational in IFS is applied to well-mixed layers only, such as the dry convective boundary layer (CBL) and the stratocumulus topped PBL. This paper presents an extension of EDMF that enables representation of conditionally unstable shallow cumulus cloud layers, thus covering all major convective boundary layer regimes. Second target of this project is to improve representation of transitions between such regimes in IFS.

Three important principles define the structure of the shallow cumulus extension. The first is the fact that the transporting cumulus updrafts are part of a joint-distribution of total specific humidity, potential temperature

and vertical velocity that is increasingly skewed with height (e.g. Wyngaard and Moeng, 1992). Any parameterization of turbulent transport requires reconstruction of this skewed distribution in some way. Theoretically, this requires knowledge of at least three of its lowest statistical moments, which can be explicitly modelled (e.g. Lappen and Randall, 2001; Golaz, 2002). An alternative method resolves skewness by means of multiple rising updrafts, each representing a separate segment (or fraction) of the joint PDF (e.g. Kain and Fritsch, 1990; Neggers et al., 2002). This technique is also applied here, however additional degrees of freedom are consciously introduced in various new ways. Key novelty is that each updraft represents an area fraction that is *flexible*, as a function of model state. This flexibility subsequently finds its way into updraft initialization at the surface. As will be shown, this method facilitates representation of transient cloudy boundary layers, and regime transitions in general.

The second defining principle is the explicit representation of the coupling between shallow cumulus clouds and the sub-cloud mixed layer (e.g. Betts, 1976; Nicholls and LeMone, 1980). Recent studies have revealed the existence of feedbacks between cumulus mass flux and the stability of the cloud base transition layer (Mapes, 2000; Bretherton et al., 2004; Neggers et al., 2004, 2006). We let the nature of this "valve" mechanism determine the area partitioning of the updraft ensemble. To this purpose we define and resolve two matching updraft groups; one group representing all dry mixed-layer updrafts that stop below cloud base, the other representing all updrafts that condense and become positively buoyant cumulus clouds. Their area fractions are parameterized, as a function of moist static stability above mixed layer top. These choices have some useful consequences. Dry and moist transporting updrafts can now coexist at any time. In combination with flexible updraft area partitioning this theoretically enables a gradual onset and decay of cumulus mass flux. By stopping below cloud base the dry updraft acts to maintain the internal counter-gradient structure of the mixed layer, as well as the temperature and humidity jumps across the transition layer. Finally, the valve mechanism thus introduced in the mass flux closure always acts to equilibrate the shallow cumulus topped PBL.

The third defining principle of the new extension is an internally consistent treatment of turbulent transport and clouds within the PBL. These are often modeled in separate schemes, which is somewhat at odds with the fact that clouds and transport in the cumuliform PBL typically refer to the same turbulent eddies, with relatively short turn-over timescales. This motivates parameterizing both PBL cloudiness and transport in terms of the same reconstructed joint-distribution, an approach demonstrated by Lappen and Randall (2001) and Golaz (2002) to enable a unified, integrated representation of subgrid transport and clouds for different regimes. To this purpose, a bimodal statistical cloud scheme (Lewellen and Yoh, 1993) is attached to the EDMF scheme, in which the total PDF is assumed to consist of two separate, independent Gaussian PDFs; one representing the active (updraft) clouds and one the passive (diffusive) clouds. As this decomposition is equivalent to that defining the EDMF framework, a bimodal PDF scheme thus forms a natural extension of EDMF into the modelling of clouds.

Part I of this paper is concerned with the formulation of the transport scheme. New model components will be evaluated individually against large eddy simulation (LES) results for prototype shallow cumulus cases, including steady state and transient scenarios. This supports the parameterizations, and allows realistic calibration of associated constants of proportionality. Particular attention will be given to diurnal cycles of shallow cumulus as observed at the ARM SGP site, motivated by the poor represenation of this scenario in IFS. Part II of this paper presents the extension of the EDMF framework into the statistical representation of sub-grid boundary layer clouds. Finally, part III presents comprehensive evaluation of the new model. Performance will be evaluated against LES and observational datasets, for i) prototype cases, ii) transitional cases, and iii) globally, when interactive with the larger scales in the IFS.

The EDMF approach is shortly introduced in sections 2 and 3. The multiple updraft component is formulated in section 4, and the diffusive component in section 5. The results are further discussed in section 6, and some concluding remarks are made in 7. Appendix A gives details of the LES code and all cases.

2 Conserved state variables

The PBL model is formulated in terms of thermodynamic state variables ϕ that are conserved for moist adiabatic motion,

$$\phi \in \{q_t, \theta_l\}. \tag{1}$$

Here q_t is the total specific humidity, defined as

$$q_t \equiv q_v + q_l + q_i, \tag{2}$$

where q_v is specific humidity, and q_l and q_i are specific liquid and ice water content respectively. The other state variable θ_l is the liquid water potential temperature,

$$\theta_l \approx \theta - \frac{L_v q_l + L_s q_i}{c_p \Pi} \tag{3}$$

where θ is potential temperature, c_p is the specific heat capacity at constant pressure, Π is the Exner function, L_v is the specific latent heat of the phase change of evaporation, and L_s that of sublimation. The grid-box average budget equation for ϕ can in short notation be written as

$$\frac{\partial \overline{\phi}}{\partial t} = -\left.\frac{\partial \rho\, \overline{w'\phi'}}{\rho\, \partial z}\right|_{\mathrm{PBL}} + \left(\frac{\partial \overline{\phi}}{\partial t}\right)_{\mathrm{Ph}} + \left(\frac{\partial \overline{\phi}}{\partial t}\right)_{\mathrm{LS}}, \tag{4}$$

where the horizontal overbar indicates a horizontal average over the gridbox, and the prime represents any perturbation from that average. ρ is air density, subcript *Ph* indicates the tendency due to all physics not related to PBL turbulence, and subscript *LS* indicates the tendency due to the larger (resolved) scales in the GCM. This paper is only concerned with the parameterization of the PBL turbulent flux $\overline{w'\phi'}$ and PBL cloud fraction and condensate. For a complete description of all other terms in the budget we refer to the IFS Cycle 31R1 documentation (available on the internet at *http://www.ecmwf.int/research/ifsdocs/*).

3 The eddy diffusivity mass flux (EDMF) framework

The multiple updraft model presented in this study is an extension to the eddy diffusivity mass flux (EDMF) framework, as formulated by Siebesma and Teixeira (2000) and Siebesma et al. (2007). The implementation in the ECMWF model is described by Köhler (2005) and Tompkins et al. (2004). Only a short summary is given in this section, for further details we refer to these papers. The remainder of this paper presents the new approaches and concepts that together form the new extension.

Ertel (1942) was among the first to address the different behaviour of turbulent transport by organized updrafts compared to that by smaller, more random perturbations. While small perturbations tend to do transport in a more diffusive manner (down-gradient), organized updrafts are able to overcome local stability and hence do transport against local gradients. This has been the motivation for representing counter-gradient transport terms alongside pure diffusive, K-diffusion terms (Holtslag and Moeng, 1991).

Motivated by these arguments a decomposition is made of the total turbulent flux $\overline{w'\phi'}$ into an advective part by organized updrafts and a diffusive part by weaker, more random perturbations,

$$\overline{w'\phi'} = \mathscr{A}^{\mathrm{up}}\, \overline{w'\phi'}^{\mathrm{up}} + \mathscr{A}^{\mathrm{K}}\, \overline{w'\phi'}^{\mathrm{K}} \tag{5}$$

where $\mathscr{A}^{\mathrm{up}}$ is the area fraction covered by the organized updrafts, and $\mathscr{A}^{\mathrm{K}} = 1 - \mathscr{A}^{\mathrm{up}}$ is that covered by the remaining, "diffusive" air. Based on the typically observed small values of the area fraction covered by

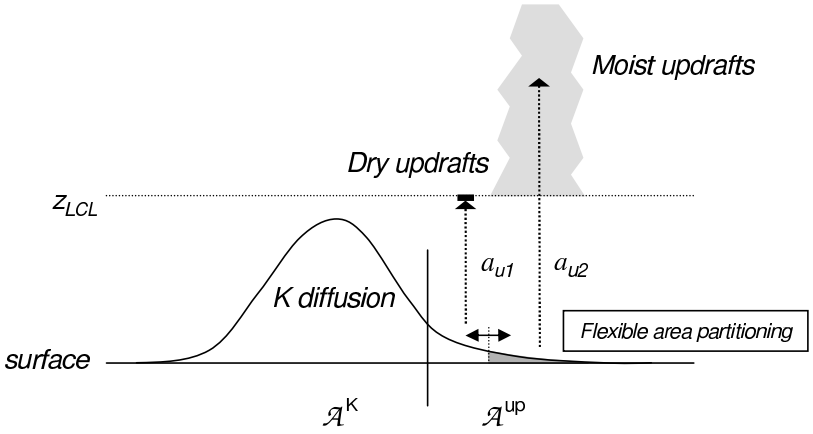

Figure 1: The eddy diffusivity mass flux (EDMF) framework for boundary layer convection, featuring multiple updrafts. $\mathcal{A}^{up}$ is the fraction explicitly represented by advective updrafts, while $\mathcal{A}^{K}$ represents diffusive motions. Fraction a_{u1} represents dry updrafts that never reach their lifting condensation level, while fraction a_{u2} represents updrafts that condense and become positively buoyant cumulus clouds (shaded grey).

organized updrafts we choose $\mathcal{A}^{\rm up} = 0.1$. The vertical transport by the smaller turbulent perturbations is represented by a down-gradient diffusive term,

$$\mathcal{A}^{\rm K}\,\overline{w'\phi'}^{\rm K} \;=\; -K_\phi\,\frac{\partial\overline{\phi}}{\partial z}. \tag{6}$$

The closure of eddy diffusivity coefficient K_ϕ is addressed in Section 5. The advective transport by organized updrafts is explicitly modeled using an ensemble mass flux model,

$$\mathcal{A}^{\rm up}\,\overline{w'\phi'}^{\rm up} \;=\; \sum_{i=1}^{I} M_{ui}\,\left(\phi_{ui}-\overline{\phi}\right), \tag{7}$$

where subscript u indicates the property of a specific updraft group (to be defined later) with i is its index number, and I is the total number of such updraft groups. M_{ui} is the collective volumetric mass flux of group i, defined as

$$M_{ui} \equiv a_{ui}\,w_{ui}. \tag{8}$$

Here a_{ui} is the area fraction covered by all updrafts in group i, with

$$\mathcal{A}^{\rm up} \;=\; \sum_{i=1}^{I} a_{ui}, \tag{9}$$

and w_{ui} is the collective vertical velocity of group i. The properties of each group are obtained from a rising plume budget model, as described in the next section. Concerning the vertical extent of the updraft model, strong observational evidence exists (e.g. LeMone and Pennell, 1976) that cumulus updrafts originate far below cloud base as dry updrafts. Accordingly, initialization is performed at the top of the surface layer, after which the updraft ensemble is allowed to rise and potentially cover the whole PBL depth. Figure 1 contains a schematic overview of the EDMF scheme featuring multiple updraft groups.

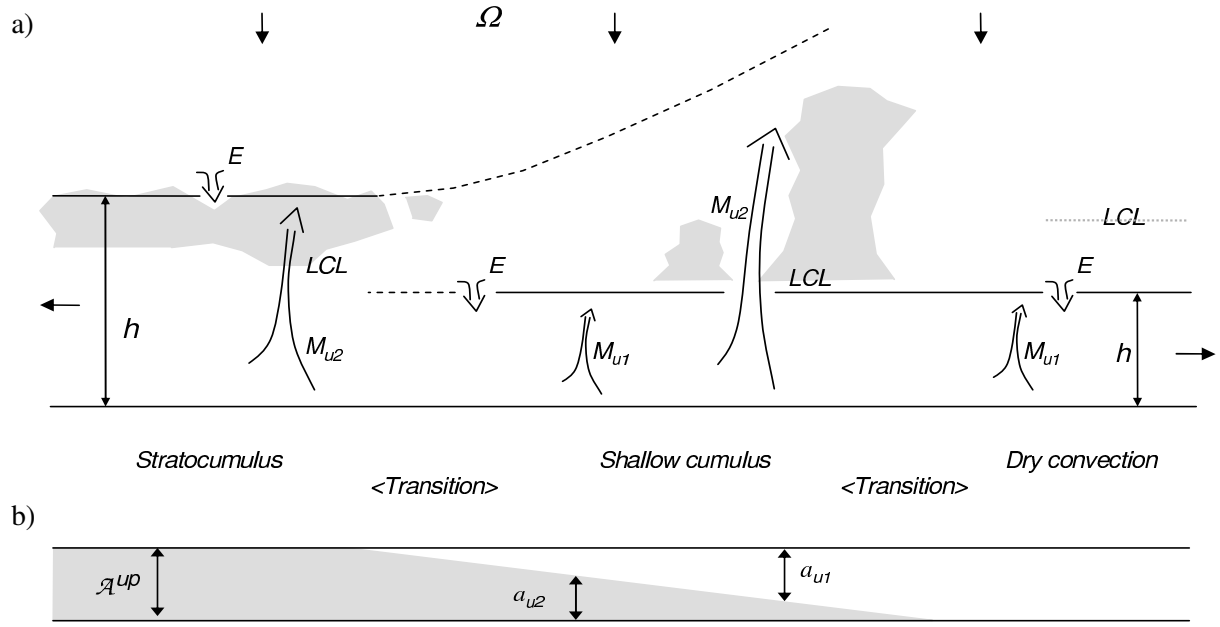

Figure 2: a) Schematic illustration of several typical regimes of PBL convection, and the transitions between them, that can be represented by the dual mass flux scheme. Included are stratocumulus (left), shallow cumulus (middle), and dry convection (right). Several terms in the mixed layer mass budget are also shown, being top entrainment E, mass flux M and low level divergence (horizontal arrows) induced by large scale vertical motion Ω (vertical arrows). b) The corresponding partitioning of the total fraction covered by organized updrafts $\mathcal{A}^{up}$ into a dry group with fraction a_{u1} and a moist group with fraction a_{u2} (shaded).

4 Transporting updrafts

4.1 A dual mass flux framework

In this model each updraft group corresponds to a certain segment (or fraction) of the sub-grid joint-PDF. The number of updraft groups I in the model still needs to be determined. How many is sufficient? Associated with this choice is the question of what each updraft should represent. Two defining choices are now made. First, to maintain computational efficiency, only a limited number of updraft groups is explicitly resolved. As a result, the updraft fractions are relatively large. Second, each updraft fraction is not assumed to be fixed in time, but is flexible, as a function of model state. This is a novelty in multiple parcel modelling.

We now argue that the explicit modelling of two basic classes of updrafts ($I = 2$) gives the scheme sufficient degrees of freedom for capturing the major PBL convective regimes, and transitions between them. One class ($u1$) represents all organized dry updrafts stopping at mixed layer top, the other ($u2$) represents all organized updrafts that condense and become positively buoyant cumulus updrafts (see Fig. 1). Figure 2 gives a schematic overview of all scenarios that can in theory be represented by this dual mass flux framework (hereafter referred to as *DualM*).

What are the benefits of this approach? First, dry and moist updrafts can coexist simultaneously. LES results reveal that advective transport by dry subcloud thermals that never manage to become moist updrafts contributes significantly to the total turbulent flux in the mixed layer (see Fig. 3). By stopping at mixed layer top, these dry updrafts are in effect maintaining the humidity and temperature jumps through the cloud base transition layer, by picking up heat and moisture close to the surface and delivering it to the top of the mixed layer.

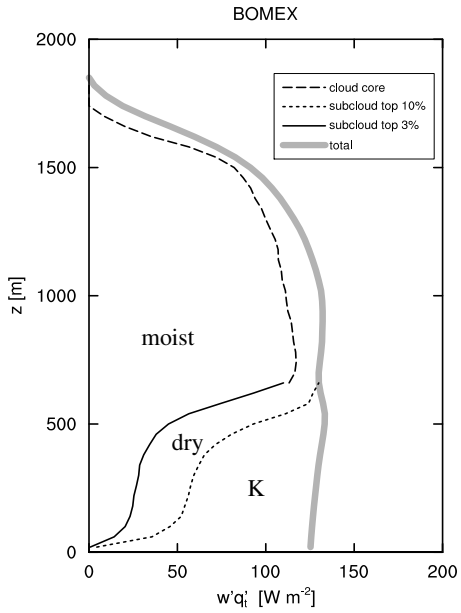

Figure 3: LES sampled decomposition of $\overline{w'q'_t}$ (thick grey) into contributions by i) subcloud updrafts that will become clouds (solid black), ii) dry subcloud updrafts that stop before reaching their LCL (dotted black) and iii) the cloud core (dashed black). The sub-cloud flux by updrafts that will become cumulus louds is obtained by assuming its fraction equal to the core fraction at cloud base (3% for this case). The dry updraft flux represents the sub-top 7%.

Simultaneously, this maintains the countergradient structure of the sub-cloud mixed layer.

Second, allowing for flexible updraft area fractions in time as a function of model state introduces an extra degree of freedom in the system of equations. As a consequence, gradual transitions from dry to shallow convection can now occur in the model, through the onset and gradual growth of cumulus mass flux as a result of a slowly increasing moist area fraction a_{u2}. On the other hand, a gradual introduction of a dry updraft stopping below cloud base is also possible, thought relevant in the process of decoupling between cloud- and mixed-layer. Allowing such "soft" transitions is a key step towards a unified representation of dry convection, shallow cumulus convection and stratocumulus convection. In all these regimes updraft transport is somehow applicable: for example, surface initialized updrafts are important in feeding stratocumulus cloud layers with humidity, thus providing the coupling of this cloud layer with the surface. The updraft area fraction is an extra free model variable, requiring parameterization. Through (8) this in effect replaces the cloud base mass flux closure relying on bulk moisture convergence that is currently used in CY31R1.

4.2 Updraft fraction closure

Any top-fraction of a unimodal PDF can be expressed as a function of the width of the PDF and the distance from the PDF-mean, a technique often used to statistically parameterize the sub-grid cloud fraction in GCMs (Sommeria and Deardorff, 1977). In principle this technique is also applicable to the positively buoyant cloud fraction (e.g. Kain and Fritsch, 1990; Siebesma and Cuijpers, 1995), which is the fraction represented by a_{u2} in this model. Using a new variance scaling for cumulus topped mixed-layers, Neggers et al. (2007) applied this technique to derive the following parameterization for a_{u2},

$$a_{u2} = \left(\frac{\Delta h}{h}\right)\frac{1}{2p+1}, \tag{10}$$

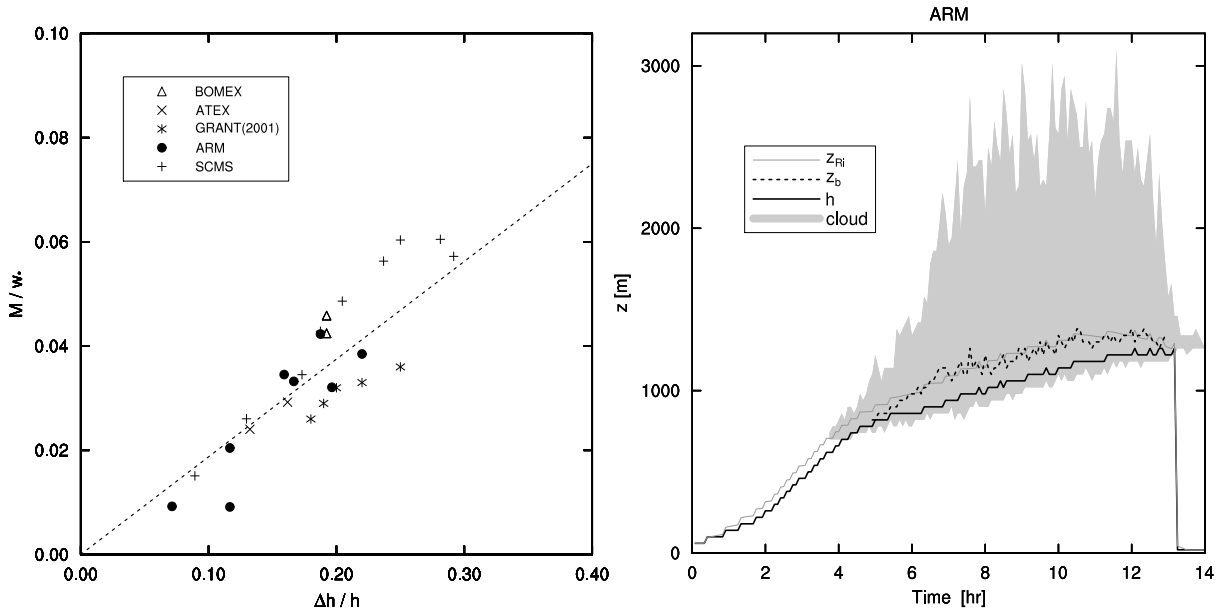

Figure 4: a) The moist convective area fraction M/w^* as a function of the ratio of transition layer depth Δh to mixed layer depth h, as diagnosed in LES. Each symbol represents an hourly average, and the symbol types refer to different shallow cumulus cases. The dotted line is the least squares linear fit. Figure copied from Neggers et al. (2007). b) Time series of the level of minimum buoyancy flux h, the level of maximum core fraction z_b, the top of the entrainment layer z_{Ri}, and the cloud layer for the ARM case, as diagnosed in LES.

where h is the depth of the mixed layer and Δh the depth of the layer between the level of minimum buoyancy flux and the level of maximum cloud core fraction. This layer is often referred to as the transition layer (e.g. Albrecht et al., 1979; Yin and Albrecht, 2000; Grant, 2001). Constant p is the shape parameter of the symmetric Beta function that was used to describe the associated PDF. Figure 4a illustrates that the existence of this relation is supported by LES results. The value $p = 2.2$ is obtained from the slope of the linear fit to this data. Figure 4b shows the opening and closing of the transition layer at the onset and decay of cumulus convection, illustrating that transition layer depth carries information on a_{u2}, which supports the use of local depth-scales in parameterization of the latter.

The double criterion of updraft condensation and positive buoyancy that defines a_{u2} is reflected in the parameterization of transition layer depth Δh, through a dependency on two depth-scales,

$$\Delta h \;=\; \mathrm{Min}\left(\Delta h_{\mathrm{Ri}},\, \Delta h_{\mathrm{cl}} \right). \tag{11}$$

The first depthscale Δh_{Ri} expresses dry stability, or the depth of the layer in which dry mixed layer thermals that are responsible for top-entrainment lose their kinetic energy (that scales with w_*^2) to negative buoyancy (Neggers et al., 2007),

$$\frac{g}{\Theta_0}\,\frac{1}{2}\,\frac{\partial \overline{\theta_v}}{\partial z}\bigg|_h \Delta h_{\mathrm{Ri}}^2 \;=\; \frac{1}{2}\,{w_*}^2, \tag{12}$$

where $\partial_z \overline{\theta_v}\big|_h$ is the local gradient of virtual potential temperature across the transition layer, and

$$w_* \;=\; \left(\frac{g}{\Theta_v^0}\, \overline{w'\theta_v'}\big|_s \; h \right)^{\frac{1}{3}}. \tag{13}$$

This layer is often referred to as the top-entrainment layer. Equation (12) can be rewritten as a dependency on

the interfacial Richardson number Ri^h,

$$\frac{\Delta h_{\mathrm{Ri}}}{h} = \frac{1}{Ri_h}, \qquad Ri^h \equiv \frac{\frac{g}{\Theta_v}\Delta\theta_v^h \, h}{{w_*}^2}. \tag{14}$$

This makes parameterization (10) commensurate with the equilibrium scaling of Stevens (2006) and the LES results of Grant (2006), both suggesting a mass flux dependence on the inverse Richardson number. The second depthscale Δh_{cl} introduces dependency on the occurrence of condensation in rising thermals at mixed layer top (Neggers et al., 2004, 2006). This *cumulus instability depthscale* is parameterized proportional to the cloudy depth of a strong, non-transporting test updraft ($i = 0, a_{u0} = 0.02$),

$$\Delta h_{\mathrm{cl}} = \gamma\left(z_{u0}^{\mathrm{top}} - z_{u0}^{\mathrm{lcl}}\right) \tag{15}$$

Figure 4b illustrates that Δh correlates well with convective cloud depth, suggesting $\gamma = 0.15$. This correlation expresses the impact of transition layer stability on the vertical velocity budget of a rising cloudy updraft, affecting the eventual height it reaches. Parameterization (15) is therefore most applicable to forced convection, in which the impact of transition layer stability on convective cloud depth is not yet obscured by latent heat release.

Stability and condensation above mixed layer top thus together determine the moist area fraction in the model. Taking the minimum of both depth-scales ensures that both criteria can constrain a_{u2}. This is illustrated in Fig. 4b, showing the time-development of both depth-scales during an LES simulation of a diurnal cycle of shallow cumulus at ARM SGP. The top of the entrainment layer z_{Ri} is obtained by vertically integrating moist static stability ($\Delta\theta_v$) above h until equation (12) is met. The depth of the entrainment layer Δh_{Ri} matches transition layer depth Δh reasonably well in the period of significant convective cloud depth. However, as Δh_{Ri} reflects the overshooting depth of *dry* thermals, it is always non-zero, also in the dry CBL. This motivates the superposition of an additional criterion reflecting updraft condensation. The main role of this depth-scale Δh_{cl} is to ensure that the moist updraft area fraction goes to zero for the dry convective limit

$$\lim_{(z_{u0}^{\mathrm{top}} - z_{u0}^{\mathrm{lcl}}) \to 0} a_{u2} = 0. \tag{16}$$

The definition of mass flux (8) means that the same limit applies to M_{u2}. Depth scale Δh_{cl} therefore reproduces potentially gradual transitions between the dry CBL and the shallow cumulus topped PBL. Numerical benefit of (15) over (12) in this respect is that cumulus depth is typically better resolved than jump $\Delta\theta_v^h$.

As w_* is typically about 1 m/s, M_{u2} will be sensitive to a_{u2}. Area fractions of only a few percent already create sufficiently large cumulus (mass)fluxes to balance the large scale forcings in the cloud layer. The dependence of a_{u2} on stability and updraft condensation thus introduces new feedbacks in the transport scheme between cumulus transport and the subcloud mixed layer. This mechanism acts to equilibrate the boundary layer, as will be illustrated in section 6.

4.3 Flexible updraft initialization

The next step is to apply the flexible area fractions of the updrafts, as parameterized in the previous section, in their surface initialization. To this purpose these fractions are assumed constant with height throughout the sub-cloud mixed layer. As a consequence, at the surface the moist fraction a_{u2} represents the fraction of the updrafts that will make it through the mixed layer and manage to condense and become buoyant cumulus clouds. A first-guess of the area fraction of buoyant cumulus updrafts at cloud base thus determines the partitioning of the updraft ensemble and its surface initialization.

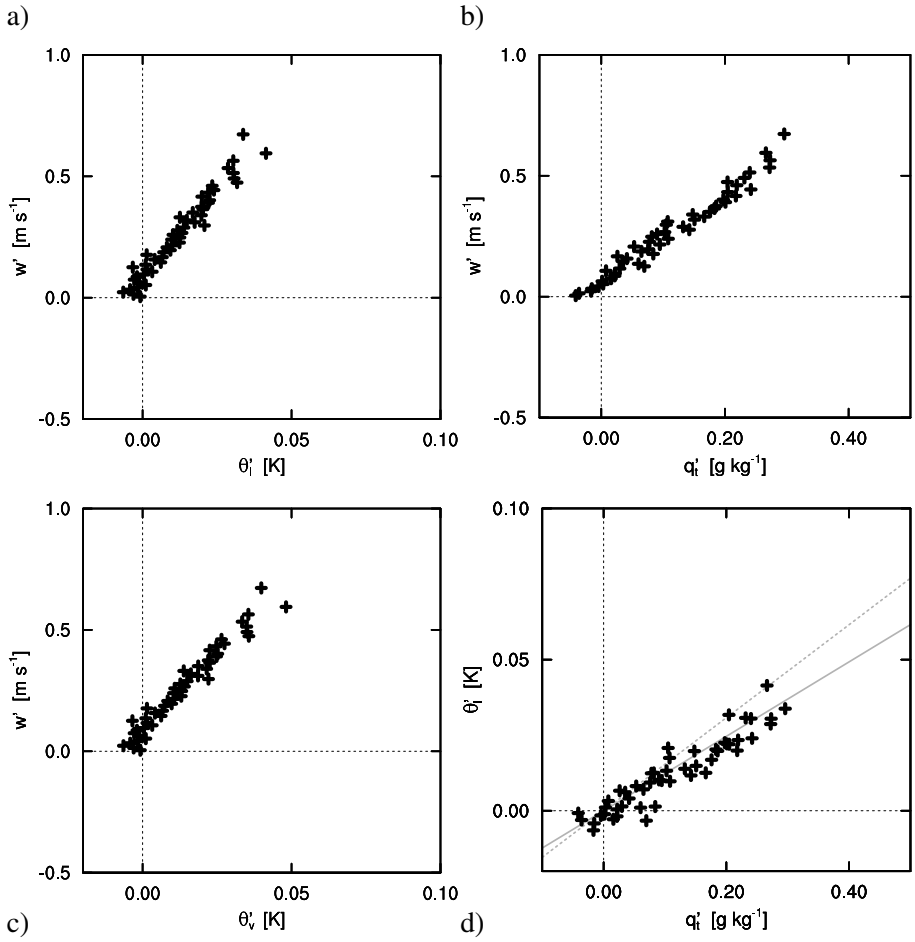

Figure 5: Scatterplots of LES updraft excesses at 60*m height during the BOMEX case. a) w versus* θ_l*, b) w versus* q_t*, c) w versus* θ_v *and d)* q_t *versus* θ_l*. Each point represents an updraft average, representing a fixed fraction of air (*1%*) in the tail of the PDF. The top* 50 *bins are plotted. The slope of the grey lines in panel d) represents the Bowen ratio* $\overline{w'\theta_l'}/\overline{w'q_t'}$*, at the surface (dotted) and at this height (solid).*

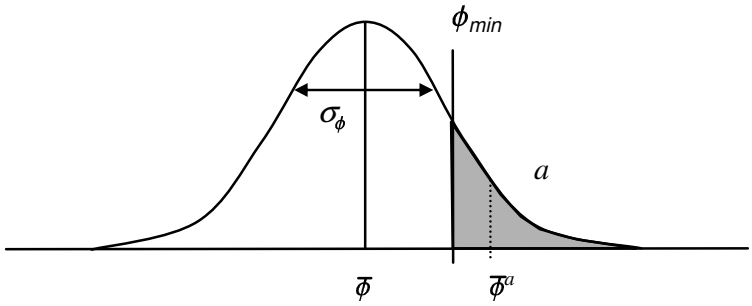

Figure 6: The PDF of the Normal distribution $N\left(\overline{\phi}, \sigma_\phi\right)$*, featuring the mean* $\overline{\phi}^a$ *(dashed line) of the updraft that covers the top percentage a (shaded).* ϕ_{min} *indicates the lower boundary of the bin.*

LES scatterplots of surface layer thermodynamic variables during BOMEX are shown in Fig. 5. Due to the averaging over a bin of 1%, the updraft average vertical velocity w^i correlates well with its temperature and moisture excess. Furthermore, in a humidity-temperature frame the perturbation points fall on the line defined by the local Bowen ratio $\overline{w'\theta_l'}/\overline{w'q_t'}$, see panel d). These results support the use of reconstructed joint-PDFs for initialization of model updrafts that represent a similar finite fraction of air.

Suppose a represents a certain top area fraction of the joint PDF that lies on the Bowen ratio line, see Fig.6. In case of a Normal distribution $N\left(\overline{\phi},\sigma_\phi\right)$ the average properties of this fraction $\overline{\phi}^a$ can be written as a unique function of the variance σ_ϕ and the fraction a,

$$\overline{\phi}^a = \overline{\phi} + \mathscr{D}(a)\ \sigma_\phi, \tag{17}$$

$$\overline{w}^a = \mathscr{D}(a)\ \sigma_w \tag{18}$$

where $\mathscr{D}(a)$ is a shape function stored in a precalculated look-up Table 2, see Appendix B. As the moist updraft fraction a_{u2} corresponds to the top fraction of the PDF, average $\phi_{u2} \equiv \overline{\phi}^{a_{u2}}$ can be obtained through (17). The dry updraft fraction a_{u1} corresponds to a sub-top fraction with initial value $\phi_{u1} = (\mathscr{A}^{\rm up}\phi_{up} - a_{u2}\phi_{u2})/a_{u1}$. The thermodynamic variances at initialization level $z^{\rm ini}$ are obtained from surface layer similarity theory,

$$\sigma_\phi(z^{\rm ini}) = \frac{\overline{w'\phi'}\big|_s}{\sigma_w(z^{\rm ini})}, \tag{19}$$

where $\sigma_w(z^{\rm ini})$ is the vertical velocity variance at initialization level (Holtslag and Moeng, 1991),

$$\sigma_w(z^{\rm ini}) \approx 1.2\left(u_*^3 + 1.5\kappa\frac{g}{\Theta_v^0}\,\overline{w'\theta_v'}\big|_s\ z^{\rm ini}\right)^{\frac{1}{3}}. \tag{20}$$

Here u_* is the friction velocity, $\kappa = 0.4$ the Von Karman constant, and $\frac{g}{\Theta_v^0}\,\overline{w'\theta_v'}\big|_s$ the surface buoyancy flux. The latter formula ensures that surface layer turbulence can be generated by wind shear, even in neutral or weakly stable conditions.

The use of flexible updraft fractions in their surface initialization introduces a more complex interaction between moist convective clouds and surface properties, compared to using constant initial updraft excesses. Given the PDF, a larger moist updraft area fraction (for example due to higher relative humidity at cloud base) implies a smaller initial updraft excess, due to the associated shift of $\overline{\phi}^a$ towards $\overline{\phi}$, see Fig.6. Updraft fraction and excess thus counteract each other in the updraft advective flux, see (7). As will be shown in the evaluation, this interaction represents a second stabilizing feedback mechanism in the PBL scheme.

4.4 Updraft budgets

As described earlier, the model updrafts are coupled to an assumed PDF at two levels, at surface initialization level and at mixed layer top. In between and above, their vertical profiles are estimated by integration of a rising plume model, described in this section. The representation of multiple updrafts requires updraft budget equations that are generally applicable enough to be able to represent different updrafts with different properties.

The updraft budget equations are in principle those as proposed by Siebesma et al. (2007). These are formulated in terms of total specific humidity and liquid water potential temperature $\phi \in \{q_t, \theta_l\}$, both conserved variables for moist adiabatic motions. Using these variables the entraining plume equation can be written as

$$\frac{\partial \phi_{ui}}{\partial z} = -\varepsilon_{ui}^{\phi}\left(\phi_{ui} - \overline{\phi}\right) + \mu_{ui}^{\phi}, \tag{21}$$

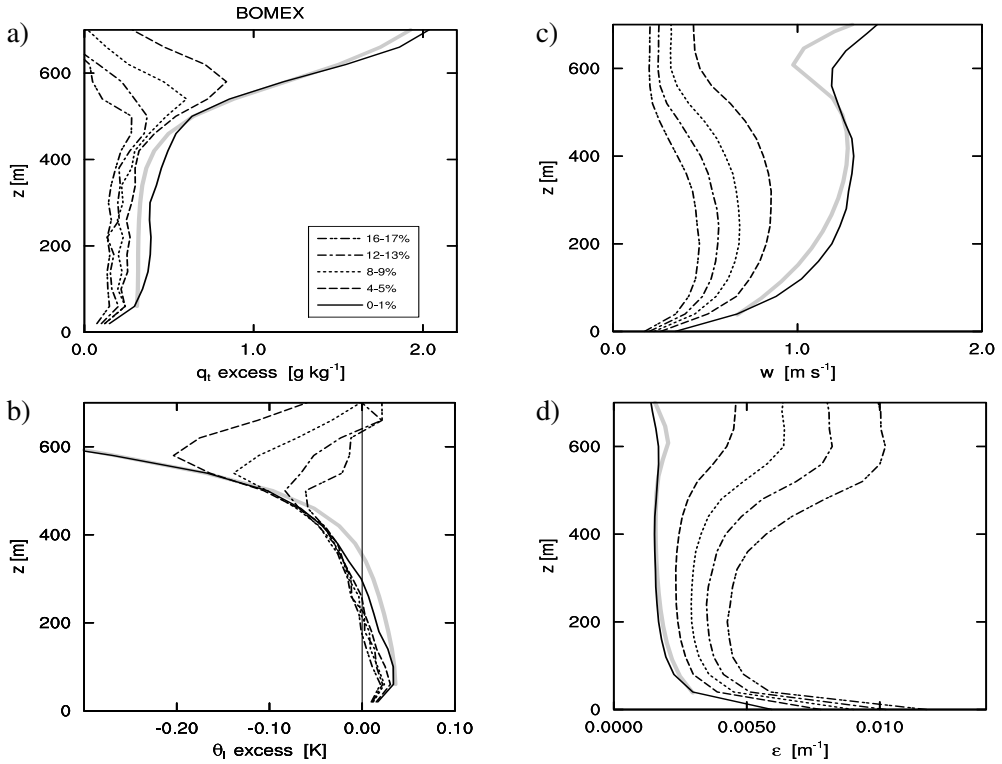

Figure 7: LES updraft properties for BOMEX, showing a) $q_{t,ui}$, b) $\theta_{l,ui}$, c) w_{ui}, and d) ε^{ϕ}_{ui} (as implied by (25) acting on w_{ui} shown in c). Each line represents an average over a 1% bin in the tail of the w-PDF, similar to Fig 5. The grey line represents the updraft budget model integrated upwards from one of the initial states. Cloud base height is 600m in BOMEX.

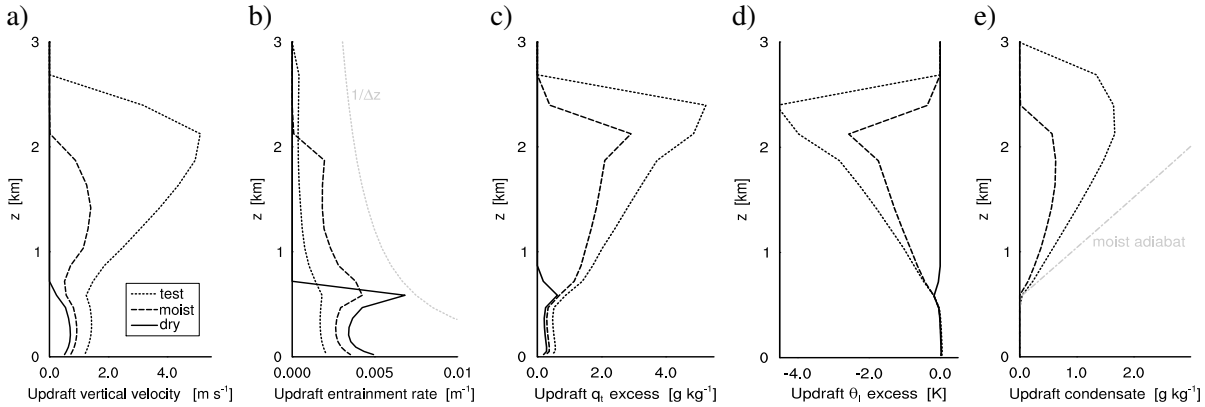

Figure 8: The updraft budget model integrated upwards from the three initial states featuring in the DualM scheme, including the dry (solid), moist (dashed) and test (dotted) updraft, for the RICO case. Shown are a) vertical velocity, b) lateral entrainment rate, excesses of c) total specific humidity q_t and d) liquid water potential temperature θ_l, and e) updraft condensate. Panel b) includes the numerical CFL criterion $1/\Delta z$ for updraft entrainment (dotted grey), and panel e) includes the moist adiabatic profile (dash dotted grey).

where ε_{ui}^{ϕ} is the thermodynamic lateral entrainment rate of updraft i, and μ_{ui}^{ϕ} represents microphysical effects, such as precipitation generation in the updraft. The updraft vertical velocity budget can be written as

$$\frac{1}{2}\frac{\partial w_{ui}^2}{\partial z} = -\varepsilon_{ui}^{w} w_{ui}^2 + B_{ui} + P_{ui}. \tag{22}$$

where P_{ui} indicates the updraft induced pressure term, assumed to be proportional to the left hand side with a factor 0.3. Kinematic entrainment is assumed to scale with thermodynamic entrainment as $\varepsilon_{ui}^{w} = 0.5\varepsilon_{ui}^{\phi}$. Budgets (21) and (22) are coupled through updraft buoyancy B_{ui}, defined as

$$B_{ui} \equiv \frac{g}{\overline{\theta_v}}\left(\theta_{v,ui} - \overline{\theta_v}\right), \tag{23}$$

which through virtual potential temperature $\theta_{v,ui}$ is a function of updraft liquid water content $q_{l,ui}$. The latter is a function of updraft saturation specific humidity $q_{s,ui}$, calculated using the triple-point method of Sommeria and Deardorff (1977). Updraft microphysics term μ_{ui}^{ϕ} is neglected for the moment, and is considered a future extension.

Interaction of updrafts with their environment is represented in system (21)-(23) in two ways. First, the entrained air directly brings in characteristics of the updraft environment, see (21). Second, updraft buoyancy over the environment at lower heights is memorized in the updraft velocity w_{ui}. The nature of lateral entrainment plays an important role in this interaction, which has motivated intensive research on this subject in the past (see Siebesma (1998) for a recent review). As opposed to constant or case-specific lateral entrainment rates we choose to use the parameterization proposed by Neggers et al. (2002). They derived lateral entrainment rates from the simplified steady-state budget of ϕ_{ui},

$$w_{ui}\frac{\partial \phi_{ui}}{\partial z} = -\frac{\phi_{ui} - \overline{\phi}}{\tau_\varepsilon}, \tag{24}$$

where the tendency due to lateral mixing is written in relaxation form, with τ_ε the time-scale typical for this process. Comparing (24) to (21) then gives

$$\varepsilon_{ui}^{\phi} = \frac{1}{\tau_\varepsilon\, w_{ui}}, \tag{25}$$

All physics behind lateral entrainment are thus embodied in adjustment timescale τ_ε, which can be argued to represent the turn-over timescale of cumulus updrafts. A recent study of cloud size statistics in LES (Neggers et al., 2002) suggests that for non-precipitating shallow cumulus this timescale, defined as cloud depth over cloud velocity, is more or less constant with eddy size, with a typical value of 400s. Such coupling of entrainment factors to updraft depth and velocity has previously been applied in the deep convection scheme of Donner (1993). More complexity could be added at a later stage by making timescale τ_ε a function of model state.

How should entrainment closure (25) be interpreted? Note that the presence of w_{ui} in (25) originates from the vertical advection term. Accordingly, this reflects that slower rising updrafts spend more time in a certain layer, thus having more time to get diluted by mixing with the surrounding air, implying a larger net entrainment rate. An alternative interpretation of this mechanism is given by substituting a constant turn-over timescale h_{ui}/w_{ui} in (25), as proposed by Siebesma (1998), which yields

$$\varepsilon_{ui} \propto \frac{1}{h_{ui}}. \tag{26}$$

This implies that smaller clouds are associated with higher entrainment rates, reflecting that the cores of bigger clouds are screened-off more effectively from the environment. Such inverse dependence on cloud size is commensurate with previous entraining plume models based on tank experiments (Turner, 1973).

Entrainment timescale τ_ε was derived from cloud population statistics. Its applicability to well-mixed layers is evaluated in Fig. 7. The vertical profiles are those connected to some of the surface PDF points as shown in Fig. 5. Comparing panels a) and c) illustrates that less diluted updrafts rise faster. Parameterization (25) captures this relation by assigning smaller entrainment rates to faster rising updrafts, see panel d). In the mixed layer the parameterized entrainment rate has a concave structure, with a distinct minimum near $z = 0.5h$. This shape is similar to the parabolic shape as found by Van Ulden and Siebesma (1997) and Siebesma et al. (2007). The question now arises if vertical integration of the updraft budget model will still reproduce this typical structure of mixed layer updrafts. All depends on the entrainment model; for example, is entrainment small enough near the surface to allow updrafts to accelerate? To answer this question, the updraft budget model is integrated offline, initialized with one of the surface points shown in Fig. 7. Despite a slight underestimation of updraft acceleration near the surface, this updraft entrainment model manages to get surface initialized updrafts to the cloud layer with realistic excesses and representative vertical structure in the mixed layer.

More impacts of flexible entrainment parameterization (25) on the model updrafts are revealed in Fig. 8, showing vertical integrations for the three initial states featuring in the DualM initialization scheme (as described in the previous section). The most striking feature is the divergence of the updraft profiles. As the same budget model is used for all updrafts, this is purely the result of i) different initialization and ii) the inverse dependence of lateral entrainment on vertical velocity, which introduces an additional coupling between equations (21)-(22). Enhanced mixing due to a smaller initial updraft velocity reduces updraft buoyancy. Through budget (22) this in turn dampens updraft velocity as it rises. Through (25) this increases the intensity of mixing even more, and so on. This positive feedback ensures that updrafts with different initial properties will get different and diverging vertical profiles. In the cloud layer, the updraft entrainment rates decrease with height, consistent with LES results (e.g. Neggers et al., 2003; Siebesma et al., 2003).

4.5 Mass transport

What remains is parameterization of the updraft mass fluxes M_{ui}. In the mixed layer, due to the assumption of constant updraft area fractions a_{ui} the mass flux M_{ui} can be obtained from equation (8) for both $i \in \{1,2\}$. As a result, within the mixed-layer the mass fluxes M_{ui} will carry the vertical structure of w_{ui}.

Above cloud base, no dry mass flux M_{u1} exists by definition. This is due to the impact of area fraction a_{u1} on the initial properties of the dry updraft, which always make it stop below cloud base (for security, this is prescribed in practice). Concerning the moist updraft, the assumption of a constant area fraction breaks down in the cloud layer, as weaker cumuli will stop at lower heights than stronger ones. Awaiting the progression from a single bulk updraft to multiple resolved moist updrafts, the shedding of mass by the moist updraft group as a whole has to be prescribed (e.g. Tiedtke, 1989),

$$\frac{1}{M_{u2}}\frac{\partial M_{u2}}{\partial z} \;=\; (\varepsilon_{u2} - \delta_{u2})\,, \tag{27}$$

where δ_{u2} is the moist updraft detrainment rate. Equation (27) is integrated bottom-up from cloud base, initialized by the value at the top of the mixed layer throughout which we assumed $M_{u2} = a_{u2} w_{u2}$.

The mass flux decay rate $(\varepsilon_{u2} - \delta_{u2})$ is parameterized as a whole, carrying several new dependencies introduced to extend its range of applicability beyond the standard Trade-wind cumulus limit (e.g. Siebesma and Cuijpers, 1995). Figure 9a shows the cloud layer mass flux in LES for several cumulus cases, normalized by its cloud base value and plotted against normalized height above cloud base. Two important characteristics can be distinguished. First, the vertical gradient of mass flux at cloud base is more or less similar in all cases. Second, a relation is suggested between the magnitude of normalized mass flux at cloud top and the relative stability of

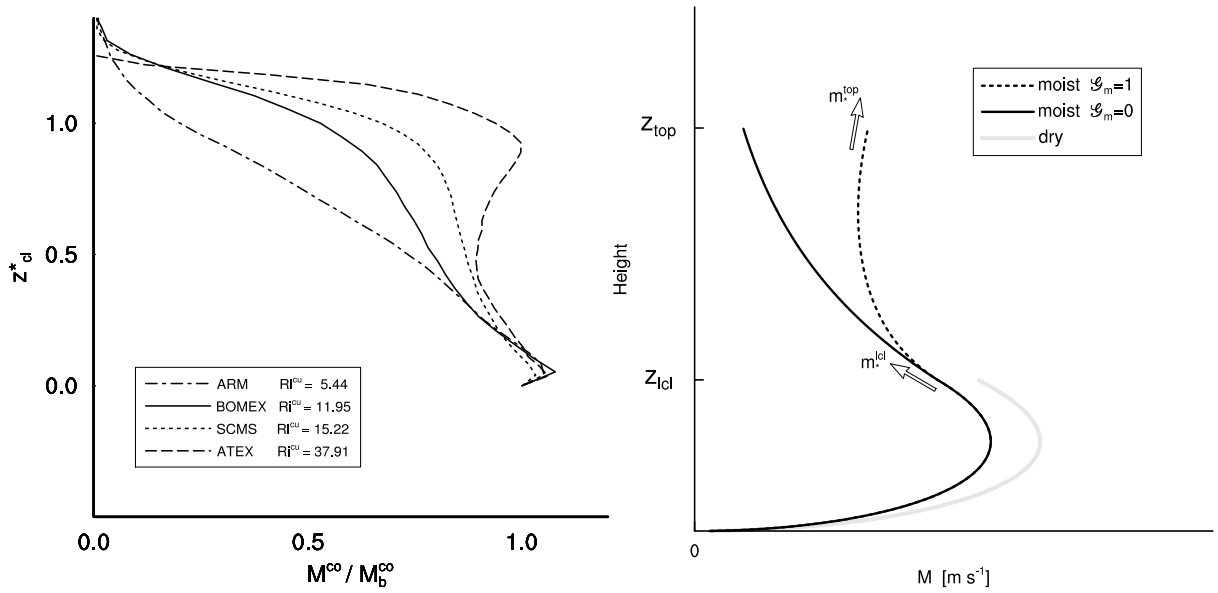

Figure 9: a) Cloud core mass flux profiles as diagnosed in LES for various cumulus cases, normalized by the cloud base value. z^*_{cl} is the height above cloud base normalized by cloud layer depth. The case acronyms are explained in Table 1. b) Configuration of the vertical structure of updraft mass fluxes in the DualM scheme. Shown are the dry updraft group ($i = 1$, grey) and the moist updraft group ($i = 2$, black), for two values of $\mathcal{G}_m$. The white arrows indicate the mass flux reduction factor at the boundaries of the bulk cloud layer (m^{lcl}_* and m^{top}_*).

the capping inversion for cumulus overshoots, as expressed by the cumulus Richardson number $Ri^{\rm cu}$,

$$Ri^{\rm cu} \equiv \frac{\Delta\overline{B}^{\rm cu}}{\langle B_{u0}\rangle}, \tag{28}$$

where $\Delta\overline{B}^{\rm cu}$ is the buoyancy jump across the interface and $\langle B_{u0}\rangle$ the cloud layer average (indicated by the brackets) buoyancy of the test updraft. This implicit dependence reflects that more stable inversions inhibit venting of PBL air into the free troposphere, which results in a more humid top half of the cumulus cloud layer. This favours more updrafts to rise further, thus reducing the decay rate of mass flux. Such dependence of mass flux on relative humidity has also been observed in cloud resolving model (CRM) simulations (Derbyshire et al., 2004), and is explained by theoretical models reflecting buoyancy sorting mechanisms (Raymond and Blyth, 1986; Kain and Fritsch, 1990).

These results motivate the following bulk parameterization. Equation (27) has an exponential solution for $M(z)$. Expressing the solution for a bulk layer in terms of a mass flux reduction factor m_*,

$$m_* \;=\; \frac{M(z+\Delta z)}{M(z)}, \tag{29}$$

then gives

$$\varepsilon_{u2} - \delta_{u2} \;=\; \frac{\ln(m_*)}{\Delta z}, \tag{30}$$

where Δz is the depth of the bulk layer. We now define Δz to be cloud layer depth, which ensures that updraft mass is distributed over the entire cloud layer, following De Rooy and Siebesma (2006). Additional flexibility is then introduced by allowing m_* to vary with height, reflecting height-dependency in the vertical gradient of mass flux. This is achieved through the following linear parameterization,

$$m_*(z) \;=\; (1-z^*_{cl})\; m^{\rm lcl}_* \;+\; z^*_{cl}\; m^{\rm top}_*, \tag{31}$$

where z^*_{cl} is height above cloud base normalized by cloud layer depth, and $m^{\rm lcl}_*$ and $m^{\rm top}_*$ are the values at the cloud layer boundaries. Based on the observed range in Fig.9a these are chosen as

$$m^{\rm lcl}_* = 0.2 \tag{32}$$
$$m^{\rm top}_* = 1.4\ \mathscr{G}_m \tag{33}$$

where factor $\mathscr{G}_m$ introduces the implicit dependency of mass flux structure on the relative stability of the capping inversion for overshooting cumuli,

$$\mathscr{G}_m = 1 - \frac{Ri^{\rm crit}}{\max(\ Ri^{\rm cu},\ Ri^{\rm crit}\ )}. \tag{34}$$

$Ri^{\rm crit}$ is a chosen critical value of $Ri^{\rm cu}$ above which inversion stability starts to affect the vertical structure of cumulus mass flux in the model. Figure 9a suggests $Ri^{\rm crit} = 5$.

Figure 9b summarizes the configuration of the vertical structure of updraft mass fluxes in the DualM scheme. The cloud layer profiles resemble those produced by the Kain and Fritsch (1990) buoyancy sorting model. The similarity between both models is that the vertical gradient of cloudy mass flux is dependent on the stability as felt by penetrating updrafts. The only difference lies in resolution and numbers; where the buoyancy sorting mechanism calculates mass flux gradients at multiple heights based on a distribution of parcels, this bulk method calculates the gradients at the layer boundaries only (cloud base and inversion), based on a single overshooting strong test parcel. In between those boundaries the bulk mass flux profile is interpolated. In the future, this parameterization could be further generalized by also making $m^{\rm lcl}_*$ flexible.

The moist updraft was introduced into EDMF to create conditionally unstable cloud layers, through the decay of its mass flux with height. This decay is now dependent on inversion stability, which as a result will affect the degree of conditional instability, as expressed by the vertical gradients of humidity and temperature in the cloud layer. This impact will be studied in section 6.

5 Diffusive transport

The configuration of the eddy-diffusivity coefficient K in the DualM scheme is similar to that in CY31R1 (Köhler, 2005), using a multiple profile method with prescribed vertical structures (Lock et al., 2000). Diffusive mixing is only applied to well-mixed layers. In that respect, the subcloud mixed layer, the dry CBL and the stratocumulus topped PBL are all treated similarly. In the shallow cumulus cloud layer no diffusion is applied, and the advective mass flux model carries all flux. However, there is one exception to this rule, and that is the cumulus inversion. In the DualM scheme, an entrainment efficiency closure is introduced through K at this height, to better describe the mixing across this potentially strong and unresolved gradient.

At both the capping inversion and at mixed layer top the diffusive flux is explicitly parameterized (overwriting the layer internal profiles), as the product of a local top-entrainment velocity and jump across the interface,

$$\overline{w'\phi'}^K_e = w_e\ \Delta\phi \tag{35}$$

where subscript e indicates the entrainment process. At mixed-layer top the entrainment velocity w^h_e is obtained using a specified ratio of top to surface buoyancy flux,

$$w^h_e = A^h \frac{\overline{w'\theta'_v}|_0}{\Delta\theta^h_v} \tag{36}$$

where A^h is a constant of proportionality, usually assumed 0.2 based on LES simulations (e.g. Stevens, 2006). At mixed layer top, an internal boundary within the cumulus PBL, mass flux exists alongside diffusion. In contrast, at the cumulus inversion only diffusive transport is allowed; the mass flux in that model-layer is replaced by a diffusive flux following (35), with the associated cumulus top-entrainment rate w_e^{cu} parameterized in a similar format as (36),

$$w_e^{cu} = A^{cu} \frac{\langle \overline{w' \theta_v'} \rangle}{\Delta \theta_v^{cu}}. \tag{37}$$

Here $\langle \overline{w' \theta_v'} \rangle$ is the cloud layer average buoyancy flux and A^{cu} is a constant of proportionality, shown by Wyant et al. (1997) to be 0.4 using CRM simulations of a stratocumulus to shallow cumulus transition. Transport by overshooting cumuli into the capping inversion layer is thus completely represented by the diffusive component of EDMF.

The similarity between (36) and (37) is that both top-entrainment rates are a function of a bulk layer average buoyancy flux and an interface buoyancy jump. Rewriting in terms of bulk Richardson numbers (14) and (28) gives

$$w_e^h = \frac{A^h}{\mathrm{Ri}^h} w_* \quad \text{and} \quad w_e^{cu} = \frac{A^{cu}}{\mathrm{Ri}^{cu}} \langle M_{u2} \rangle \tag{38}$$

respectively, where $\langle M_{u2} \rangle$ is the cloud layer average mass flux. These inverse Richardson numbers act as *entrainment efficiencies*, limiting the entrainment rate when local inversion stability $\Delta\theta_v$ gets effective in reducing the kinetic energy of overshooting updrafts. Such techniques show better skill than advective-type models in reproducing transport in strong, unresolved inversions. We thus make full use of the possibility offered by EDMF to combine diffusive and advective transport, emphasizing the representation of one of the two whenever this is numerically or conceptionally desirable.

6 Discussion

For a comprehensive evaluation of the DualM scheme we refer to Part III of this study. However, some key impacts of new model components will now briefly be assessed using the single column model (SCM) setup. Simulations of some prototype shallow cumulus cases are performed during which the cloud scheme is switched off, giving insight into the behaviour of the transport model alone. The small cloud fraction and condensate values typical of shallow cumulus convection have relatively little impact on the radiative budget, which justifies this method. In these simulations the updraft buoyancy term is the only place where condensation has an impact.

First the parameterization of the moist updraft area fraction a_{u2} is evaluated for two very different shallow cumulus scenarios; a forced shallow cumulus case (ARM SGP) and a free convective shallow cumulus case (RICO). The vertical structure of both cases is reproduced satisfactorily by the transport scheme, see Fig. 10. The degree of convective freedom is reflected in cloud layer depth, which in the RICO case is much deeper as in the ARM case. Figure 10 shows timeseries of depth-scales Δh_{cl} and Δh_{Ri} for both scenarios. One could use the criterion $\Delta h_{Ri} < \Delta h_{cl}$ as the definition of *free cumulus convection*. In the forced case, Δh_{cl} never manages to become larger than Δh_{Ri}, and thus limits a_{u2}. This shows that the system always remains close to the dry convective limit (16). The benefit of Δh_{cl} is that moist updraft depth is well resolved, ensuring gradual transitions from dry to moist convection, as illustrated by the slow increase and decrease of a_{u2} at cloud layer onset and decay in Fig. 10a. In the free convective case, Δh_{Ri} limits a_{u2}. In this scenario the cloudy depth of the updraft no longer uniquely reflects transition layer impacts on updraft buoyancy, as these get overshadowed by the impact of latent heat release in deeper cloud layers. Taking the minimum of both depth-scales thus ensures that the most appropriate scale is automatically chosen.

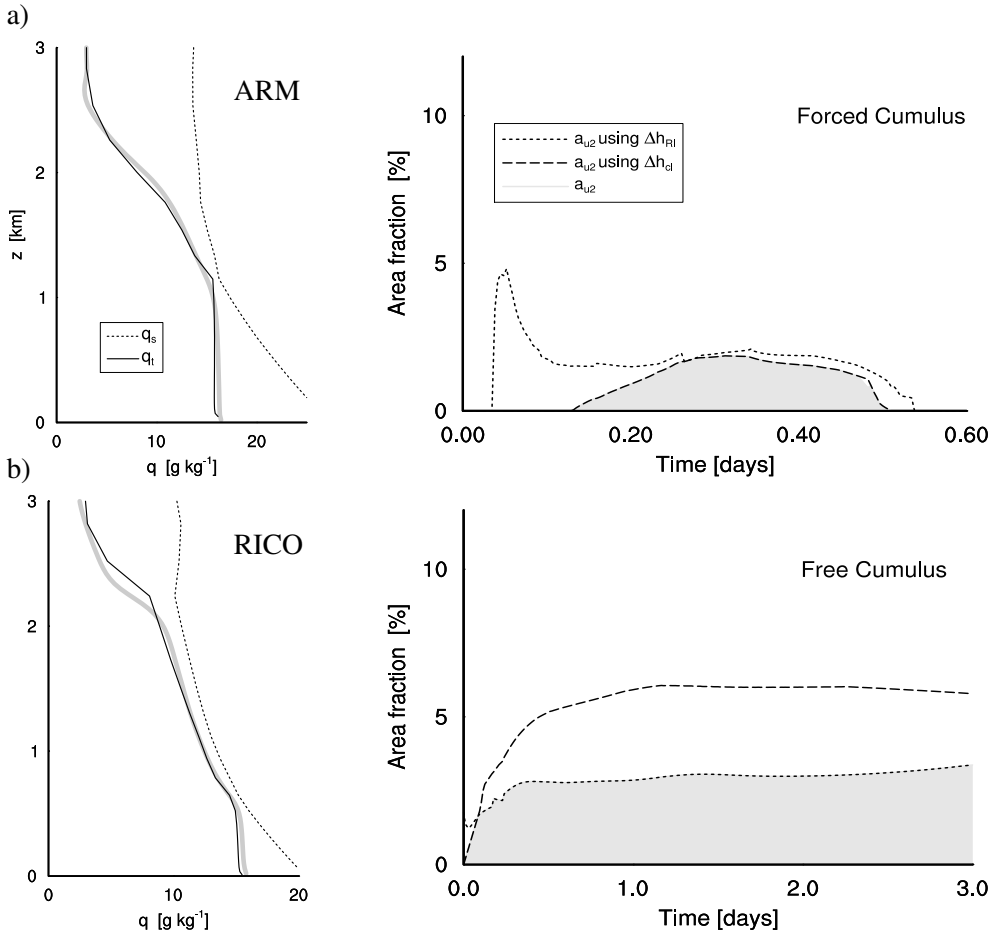

Figure 10: The left panels show vertical profiles of total specific humidity $\overline{q_t}$ (solid black) and saturation specific humidity $q_s(\overline{T})$ (dotted black) of SCM simulations of a) the ARM SGP case representing forced shallow cumulus and b) the RICO case representing free convective shallow cumulus. The corresponding LES results are plotted in thick grey. The cloud layer is recognizable as the layer in which q_t is closest to q_s. The right panels show time series of the area fractions associated with the two depth-scales Δh_{cl} and Δh_{Ri} (dashed and dotted). Their minimum (shaded grey) corresponds to the moist updraft area fraction a_{u2}.

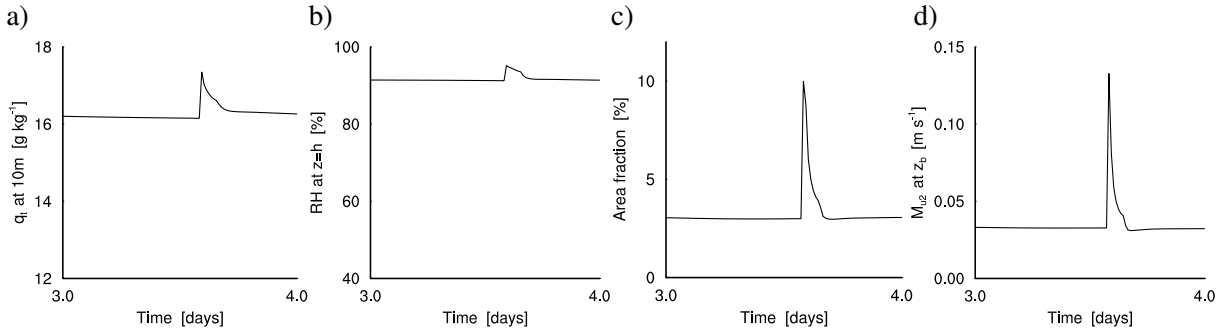

Figure 11: Same as Fig.10b, but now showing impacts of a perturbation of subcloud mixed layer humidity of $+1$ g kg^{-1}. Various quantities involved in the equilibration of the shallow cumulus topped boundary layer are shown; a) q_t at the lowest model level, b) relative humidity at mixed layer top $z = h$, c) the moist updraft area fraction a_{u2}, and d) associated updraft mass flux M_{u2}.

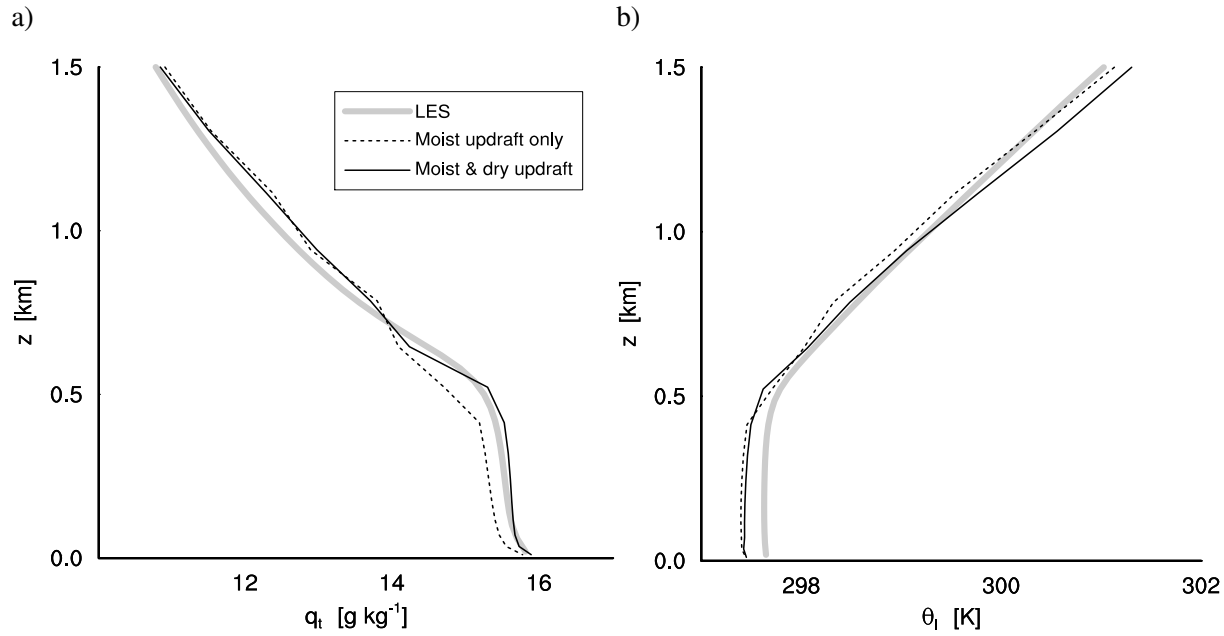

Figure 12: Comparison of the vertical structure of the subcloud mixed layer and lower cloud layer for the RICO case, showing a) total specific humidity $\overline{q_t}$ and b) liquid water potential temperature $\overline{\theta_l}$. The solid black line indicates a simulation with the standard dual mass flux setup, the dotted black line indicates a simulation with the dry updraft switched off. LES results are plotted in grey.

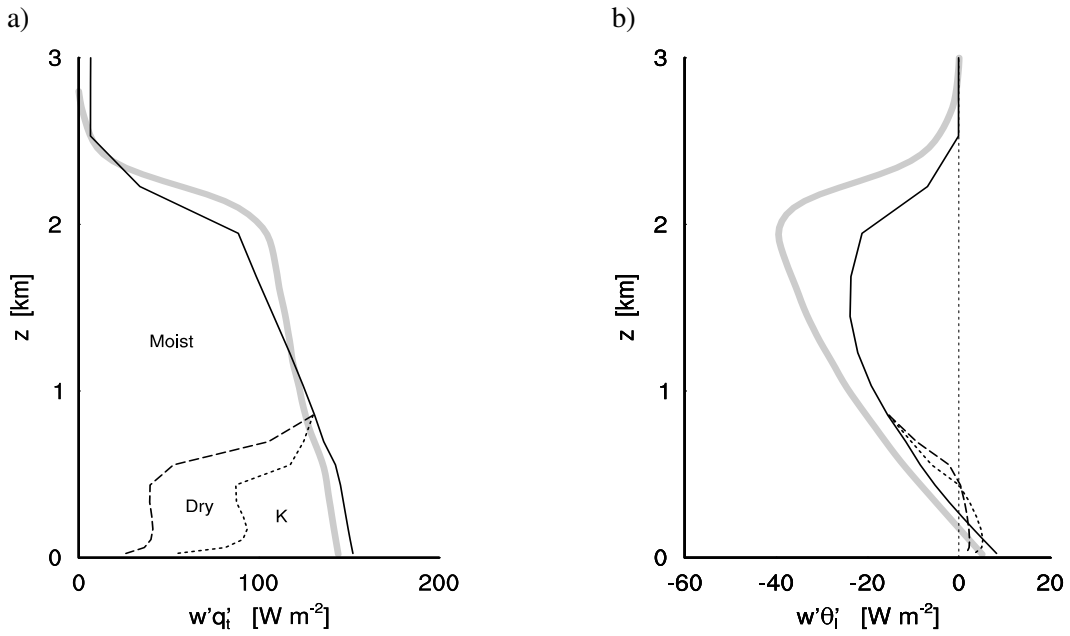

Figure 13: Turbulent fluxes of a) total specific humidity $\overline{q_t}$ and b) liquid water potential temperature $\overline{\theta_l}$ as generated by the DualM scheme for the RICO case. Individual contributions by the moist updraft (dashed line), dry updraft (between dashed and dotted lines) and diffusion (between dotted and solid lines) are indicated. LES results are plotted in grey.

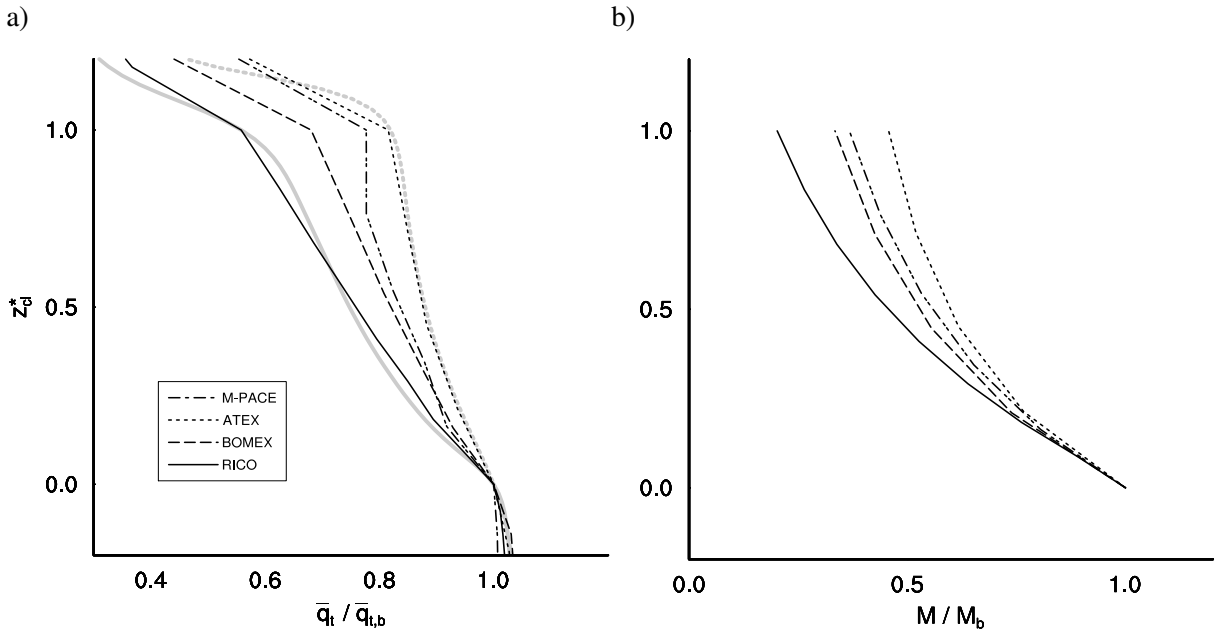

Figure 14: SCM cloud layer vertical structure of a) mean total specific humidity $\overline{q_t}$ and b) moist updraft mass flux M_{u2} for various cases, normalized by their cloud base value (subscript b). z^*_{cl} is the height above cloud base normalized by cloud layer depth. Corresponding LES profiles are shown in thick grey.

Boundary layer equilibration is assessed through a stability analysis for the RICO case. After equilibrium is reached the specific humidity of the subcloud mixed layer is artificually perturbed by $+1$ g kg^{-1} (e.g. Neggers et al., 2006), see Fig.11a. The results show that subsequently the system quickly returns to the same equilibrium state as before the perturbation, characterized by a close proximity to saturation at mixed layer top (see Fig.11b). The high relative humidity of this equilibrium state, as well as the short time-scale of re-equilibration, can be explained by the dependence of moist updraft mass flux on its flexible area fraction. This dependence first implies that condensation of updrafts is required to get a_{u2} off zero, explaining the close proximity to saturation. Second, the high sensitivity of this dependence introduces a negative feedback mechanism between cumulus mass flux and moist stability at mixed layer top (e.g. Mapes, 2000; Bretherton et al., 2004; Neggers et al., 2004, 2006). A higher relative humidity at mixed layer top is efficient in increasing the moist updraft area fraction, see Fig.11c. This directly implies a significantly larger cumulus mass flux (see Fig.11d), which acts to quickly dry out the mixed layer again, and hence to reduce itself to its previous (equilibrium) value.

Various impacts of the updraft configuration on the structure of the boundary layer are studied. The role of the dry transporting updraft within the mixed layer is examined in Figure 12. Comparing an SCM simulation with and without this dry updraft illustrates that it acts to maintain the "jumps" in $\overline{q_t}$ and $\overline{\theta_l}$ at cloud base, by depositing air of high humidity and low temperature just below mixed layer top. This also enhances the counter-gradient structure of the mixed layer (Holtslag and Moeng, 1991). Without this transport, the jumps at cloud base are significantly less pronounced. Figure 13 further illustrates the contribution of each EDMF component to the turbulent flux. Comparison to Fig.3 shows that the resulting structure of transport is realistic.

The capability of the moist updraft to generate conditionally unstable cloud layers is evaluated in Fig. 14. In this model the vertical structure of the moist updraft mass flux in the cloud layer is adaptive, dependent on inversion stability for overshooting updrafts as expressed by the cumulus Richardson number Ri_{cu}, see (31). The results illustrate that a more slowly decaying moist updraft mass flux indeed acts to create mean thermodynamic state profiles that are steeper. For stronger inversions, more updraft mass is transported to the top half of the

cloud layer, resulting in a smaller $\overline{q_t}$ gradient. This feature is in accordance with LES results. Such stronger convergence of specific humidity flux below the inversion favours formation of capping stratus layers, enabling representation of scenarios featuring cumuli rising into stratocumulus. This will be further explored in Part II of this paper.

7 Concluding remarks

In this study the complexity of the EDMF framework is enhanced to allow representation of more complex PBL scenario's. A set of modifications is proposed, argued to introduce sufficient extra degrees of freedom to represent shallow cumulus convection, and transitions to and from this PBL regime. The most important modification is the introduction of multiple updrafts. The moist updraft is configured to enable representation of conditionally unstable cloud layers that are flexibly rooted in the subcloud mixed layer. Rooting is represented through flexible updraft i) area fraction and ii) surface initialization, both a function of model state. The properties of the air transported out of the mixed layer by the cumulus updraft are affected by the mixed layer through lateral entrainment, which through an inverse dependence on vertical velocity introduces strong sensitivity to the updraft environment. The degree of conditional instability of the cloud layer is controlled by the stability of the capping inversion for overshooting updrafts, through an adaptive vertical structure of moist updraft mass flux. Finally, it is demonstrated that the multiple updraft framework facilitates representation of moist convective inhibition mechanisms.

The diurnal cycle of shallow cumulus over land has played a key role in the formulation of this model. Within 24 hours the boundary layer goes through various very different phases; first a stable situation at dawn, followed by a dry convective period, followed by forced shallow cumulus developing into free convective shallow cumulus, and finally back to a slowly re-stabilizing residual PBL after dusk. The transience of such complex scenarios requires sufficient model complexity to allow its representation. This illustrates the important role that observational data such as provided by the ARM program can play in model development, from supporting LES/CRM simulations, via evaluation of parameterizations at physics level and their subsequent improvement, to evaluation of model climate of GCMs.

The extension of the EDMF framework into the statistical modelling of boundary layer clouds and condensate is presented in Part II of this paper. Among others, the benefits of an internally consistent, bimodal treatment of transport and clouds are discussed, illustrated by model evaluation for complex PBL cloud scenarios. Finally, Part III presents a comprehensive evaluation of the full DualM scheme, for prototype cases (both steady state and transient) as well as in interactive mode with the larger scales in IFS.

Acknowledgments While affiliated at ECMWF the first author was sponsored by the Atmospheric Radiation Measurement (ARM) Program of the United States Department of Energy (DOE). We would like to thank the boundary-layer research group at the Royal Netherlands Meteorological Institute (KNMI) for supplying the LES data on the RICO case, and for many useful discussions. We furthermore thank various members of staff at ECMWF for their support and insights during the development of this model.

APPENDIX A Prototype cumulus cases

ARM SGP Atmospheric Radiation Measurement program - Southern Great Plains site *Stokes and Schwartz (1994), Ackerman and Stokes (2003)* *Brown et al. (2002)*
ATEX Atlantic Trade-wind Experiment *Augstein et al. (1973, 1974)* *Stevens et al. (2001)*
BOMEX Barbados Oceanographic and Meteorological Experiment *Holland and Rasmusson (1973), Nitta and Esbensen (1974)* *Siebesma et al. (2003)*
M-PACE period B Mixed-Phase Arctic Cloud Experiment *Harrington and Verlinde (2004), Verlinde et al. (2005)* *Xie et al. (2006)*
RICO composite Rain in Cumulus over the Ocean experiment *To be published* *http://www.knmi.nl/samenw/rico/*
SCMS Small Cumulus Microphysics Study *Knight and Miller (1998), French et al. (1999)* *Neggers et al. (2003)*

Table 1: Summary of prototype PBL cases developed for LES, documenting (in row-order) i) the case acronym, ii) its full name, iii) publications describing the field-experiment and iv) publications describing the LES case setup. The KNMI LES model is described in detail by Cuijpers and Duynkerke (1993).

APPENDIX B Precalculated functions

a	$\mathscr{D}(a)$	a	$\mathscr{D}(a)$
10^{-4}	3.958	0.1	1.754
10^{-3}	3.368	0.2	1.400
0.01	2.673	0.3	1.159
0.02	2.425	0.4	0.966
0.03	2.267	0.5	0.798
0.04	2.153	0.6	0.644
0.05	2.062	0.7	0.497
0.06	1.985	0.8	0.350
0.07	1.918	0.9	0.195
0.08	1.859	0.999	0.003
0.09	1.804	1.	0

Table 2: Gaussian shape function $\mathscr{D}(a)$ expressing the mean of the top segment of a Normal distribution $N\left(\overline{\phi}=0,\sigma_\phi=1\right)$ with area fraction a.

References

Ackerman, T. P., and G. M. Stokes, 2003: The Atmospheric Radiation Measurement program. *Phys. Today*, **56**, 38-44.

Albrecht, B. A., A. K. Betts, W. H. Schubert and S. K. Cox, 1979: A model of the thermodynamic structure of the Trade-wind boundary layer. Part I: Theoretical formulation and sensitivity tests. *J. Atmos. Sci.*, **36**, 73-89.

Augstein, E., H. Riehl, F. Ostapoff and V. Wagner, 1973: Mass and energy transports in an undistrubed Atlantic trade-wind flow. *Mon. Wea. Rev.*, **101**, 101-111.

Augstein, E., H. Schmidt and V. Wagner, 1974: The vertical structure of the atmospheric planetary boundary layer in undistrubed Trade winds over the Atlantic Ocean. *Bound.-Layer Meteor.*, **6**, 129-150.

Betts, A. K. and Jakob, C. 2002: Evaluation of the diurnal cycle of precipitation, surface thermodynamics, and surface fluxes in the ECMWF model using LBA data. *J. Geophys. Res.*, **107**(D20), doi: 10.1029/2001JD000427.

Betts, A. K., 1976: Modeling sub-cloud layer structure and interaction with a shallow cumulus layer. *J. Atmos. Sci.*, **33**, 2363-2382.

Bretherton, C. S., J. R. McCaa and H. Grenier, 2004: A new parameterization for shallow cumulus convection and its application to marine subtropical cloud-topped boundary layers. Part I: Description and 1D results. *Mon. Wea. Rev.*, **132**, 864-882.

Brown, A. R., and Co-authors, 2002: Large-eddy simulation of the diurnal cycle of shallow cumulus convection over land. *Quart. J. Roy. Met. Soc.*, **128**, 1075-1094.

Cheinet, S., A. Beljaars, M. Köhler, J.-J. Morcrette, and P. Viterbo, 2004: Assessing physical processes in the ECMWF model forecasts through the ARM SGP site measurements. *ECMWF Technical Memorandum No.?, October 2004*

Cuijpers, J. W. M., and P. G. Duynkerke, 1993: Large-eddy simulation of trade-wind cumulus clouds. *J. Atmos. Sci.*, **50**, 3894-3908.

Derbyshire, S. H., and Co-authors, 2004: Sensitivity of moist convection to environmental humidity. *Q. J. Roy. Met. Soc.*, **130**, 3055-3079.

Donner, L. J., 1993: A cumulus parameterization including mass fluxes, vertical momentum dynamics, and mesoscale effects. *J. Atmos. Sci.*, **50**, 889-906.

Ertel, H., 1942: Der vertikale Turbulenz-Wärmestrom in der Atmospähre. *Meteor. Z.*, **59**, 1690-1698.

French, J. R., G. Vali and R. D. Kelly, 1999: Evolution of small cumulus clouds in Florida: observations of pulsating growth. *Atmospheric Research*, **52**, 143-165.

Golaz, J.-C., V. E. Larson and W. R. Cotton, 2002: A PDF-based model for boundary layer clouds. Part I: method and model description. *J. Atmos. Sci.*, **59**, 3540-3551.

Grant, A. L. M., 2001: Cloud-base fluxes in the cumulus-capped boundary layer. *Quart. J. Roy. Met. Soc.*, **127**, 407-421.

Grant, A. L. M., 2006: The cumulus-capped boundary layer. II:Interface fluxes. *Quart. J. Roy. Met. Soc.*, **132**, 1405-1422.

Harrington, J., and J. Verlinde, 2004: Mixed-phase Arctic Clouds Experiment (M-PACE): The ARM scientific overview document. *Report, U.S. Dep. of Energy, Washington, D. C.*, 20 pp.

Holland, J. Z., and E. M. Rasmusson, 1973: Measurement of atmospheric mass, energy and momentum budgets over a 500-kilometer square of tropical ocean. *Mon. Wea. Rev.*, **101**, 44-55.

Holtslag, A. A. M., and C.-H. Moeng, 1991: Eddy diffusivity and countergradient transport in the convective atmospheric boundary layer. *J. Atmos. Sci.*, **48**, 1690-1698.

Kain, J. S. and J. M. Fritsch, 1990: A one-dimensional entraining/detraining plume model and its application in convective parameterizations. *J. Atmos. Sci.*, **47**, 2784-2802.

Klein, S. A., and D. L. Hartmann, 1993: The seasonal cycle of low stratiform clouds. *J. Clim.*, **6**, 1587-1606.

Köhler, M., 2005: Improved prediction of boundary layer clouds. *ECMWF Newsletter*, No. **104**, 18-22.

Knight, C. A. and L. J. Miller, 1998: Early radar echoes from small, warm cumulus: Bragg and hydrometeor scattering. *J. Atmos. Sci.*, **55**, 2974-2992.

Lappen, C.-L., and D. A. Randall, 2001: Toward a unified parameterization of the boundary layer and moist convection. Part I: A new type of mass-flux model. *J. Atmos. Sci.*, **58**, 2021-2036.

Larson, V. E., R. Wood, P. R. Field, J.-C. Golaz, T. H. Vonder Haar, and W. R. Cotton, 2001: Small-scale and mesoscale variability of scalars in cloudy boundary layers: One-dimensional probability density functions. *J. Atmos. Sci.*, **58**, 1978-1994.

LeMone, M. A., and Pennell, W. T., 1976: The relationship of Trade wind cumulus distribution to subcloud layer fluxes and structure. *Mon. Wea. Rev.*, **104**, 524-539.

Lewellen, W. S., and S. Yoh, 1993: Binormal model of ensemble partial cloudiness. *J. Atmos. Sci.*, **50**, 1228-1237.

Lock, A. P., A. R. Brown, M. R. Bush, G. M. Martin, and R. N. B. Smith, 2000: A new boundary layer mixing scheme. Part I: Scheme description and single-column model tests. *Mon. Wea. Rev.*, **128**, 3187-3199.

Mace, G. G., C. Jakob, and K. P. Moran, 1998: Validation of hydrometeor occurrence predicted by the ECMWF model using millimeter wave radar data. *Geophys. Res. Letters*, **25**, 1645-1648.

Mapes, B. E., 2000: Convective inhibition, subgrid-scale triggering energy, and stratiform instability in a toy tropical wave model. *J. Atmos. Sci.*, **57**, 1515-1535

Neggers, R. A. J., A. P. Siebesma and H. J. J. Jonker, 2002: A multi parcel model for shallow cumulus convection. *J. Atmos. Sci.*, **59**, 1655-1668.

Neggers, R. A. J., P. G. Duynkerke, S. M. A. Rodts, 2003: Shallow cumulus convection: a validation of large-eddy simulation against aircraft and Landsat observations. *Q. J. Roy. Met. Soc.*, **129**, p2671-2696.

Neggers, R. A. J., A. P. Siebesma, G. Lenderink and A. A. M. Holtslag. 2004: An evaluation of mass flux closures for diurnal cycles of shallow cumulus. *Mon. Wea. Rev.*, **132**, p2525-2538.

Neggers, R. A. J., B. Stevens, and J. D. Neelin, 2006a: A simple equilibrium model for shallow cumulus topped mixed layers. *Theoret. Comput. Fluid Dynamics*, **20**, 305-322. DOI 10.1007/s00162-006-0030-1.

Neggers, R. A. J., B. Stevens, and J. D. Neelin, 2007: Variance scaling in shallow cumulus topped mixed layers. *Accepted for publication in the Q. J. Roy. Met. Soc, February 2007.*

Nicholls, S., and M. A. LeMone, 1980: The fair weather boundary layer in GATE: the relationship of subcloud fluxes and structure to the distribution and enhancement of cumulus clouds. *J. Atmos. Sci.*, **37**, 2051-2067.

Nitta, T. and S. Esbensen, 1974: Heat and moisture budget analyses using BOMEX data. *Mon. Wea. Rev.*, **102**, 17-28.

Raymond, D. J., and A. M. Blyth, 1986: A stochastic mixing model for non-precipitating cumulus clouds. *J. Atmos. Sci.*, **43**, 2708-2718.

Rooy, W. C. de, and A. P. Siebesma, 2006: A simple parameterization for detrainment in shallow cumulus. *17th Symposium on Boundary Layers and Turbulence, 22/5/2006-26/5/2006, San Diego, AMS (int.).*

Schumann, U., and C.-H. Moeng, 1991: Plume budgets in clear and cloudy convective boundary layers. *J. Atmos. Sci.*, **48**, 1758-1770.

Siebesma, A. P., and J. W. M. Cuijpers, 1995: Evaluation of parametric assumptions for shallow cumulus convection. *J. Atmos. Sci.*, **52**, 650-666.

Siebesma, A. P., 1998: Shallow cumulus convection. *Buoyant Convection in Geophysical Flows*, E. J. Plate, E. E. Fedorovich, D. X. Viegas and J. C. Wyngaard, Eds., Kluwer Academic Publishers, 441-486.

Siebesma, A. P., and Co-authors, 2003: A large eddy simulation intercomparison study of shallow cumulus convection. *J. Atmos.Sci.*, **60**, 1201-1219.

Siebesma, A. P., and J. Teixeira, 2000: An advection-diffusion scheme for the convective boundary layer: description and 1D-results. *Proceedings of the 14th Symposium on Boundary Layer and Turbulence of the American Meteorological Society*, 133-140.

Siebesma, A. P., and Co-authors, 2004: Cloud representation in general-circulation models over the northern Pacific Ocean: A EUROCS intercomparison study. *Q. J. Roy. Met. Soc.*, **130**, p3245-3267.

Siebesma, A. P., P. M. M. Soares, and J. Teixeira: A combined eddy diffusivity mass flux approach for parameterizing turbulent transport in the convective boundary layer. *Submitted to the J. Atmos. Sci., 2007*

Sommeria, G., and J. W. Deardorff, 1977: Subgrid-scale condensation in models of non-precipitating clouds. *J. Atmos. Sci.*, **34**, 344-355.

Stevens, B., and Co-authors, 2001: Simulations of Trade-wind cumuli under a strong inversion. *J. Atmos. Sci.*, **58**, 1870-1891.

Stevens, B., 2006: Boundary layer concepts for simplified models of tropical dynamics. *Theoret. Comput. Fluid Dynamics*, **20**, 279-304.

Stokes, G. M., and S. E. Schwartz, 1994: The Atmospheric Radiation Measurement (ARM) program: programmatic background and design of the cloud and radiation test bed. *Bull. Amer. Meteor. Soc.*, **75**, 1201-1222.

Tiedtke, M., W. A. Heckley and J. Slingo, 1988: Tropical forecasting at ECMWF: The influence of physical parameterizations on the mean structure of forecasts and analyses. *Quart. J. Roy. Met. Soc.*, **114**, 639-665.

Tiedtke, M., 1989: A comprehensive mass flux scheme for cumulus parameterization in large-scale models. *Mon. Wea. Rev.*, **117**, 1779-1800.

Tiedtke, M., 1993: Representation of clouds in large-scale models. *Mon. Wea. Rev.*, **121**, 3040-3061.

Tompkins, A., and Co-authors, 2004: Moist physical processes in the IFS: Progress and plans. *ECMWF technical memorandum*, 452pp.

Turner, 1973: *Buoyancy effects in fluids.* Cambridge University Press, 367pp.

van Ulden, A. P., and A. P. Siebesma, 1997: A model for strong updrafts in the convective boundary layer. *Proceedings of the 12th Symposium on Boundary Layers and Turbulence, Aspen, USA*, American Meteorological Society, p257-259.

Verlinde, J., et al., 2005: Overview of the Mixed-Phase Arctic Cloud Experiment (M-PACE). *Proceedings of the 85th Annual Conference of the Am. Meteorol. Soc., San Diego, Ca.*.

Wyant, M. C., C. S. Bretherton, H. A. Rand, and D. E. Stevens, 1997: Numerical simulations and a conceptual model of the stratocumulus to trade cumulus transition. *J. Atmos. Sci.*, **54**, 168-192.

Wyngaard, J. C., and C.-H. Moeng, 1992: Parameterizing turbulent diffusion through the joint probability density. *Bound.-Layer Meteor.*, **60**, 1-13.

Xie, S., S. A. Klein, M. Zhang, J. J. Yio, R. T. Cederwall, and R. McCoy, 2006: Developing large-scale forcing data for single-column and cloud-resolving models from the Mixed-Phase Arctic Cloud Experiment. *J. Geophys. Res.*, **111**, D19104, doi:10.1029/2005JD006950.

Yin, B., and B. A. Albrecht, 2000: Spatial variability of atmospheric boundary layer structure over the eastern equatorial Pacific. *J. Clim.*, **13**, 1574-1592.